

Content-adaptive generation and parallel compositing of volumetric depth images for responsive visualization of large volume data

Aryaman Gupta*
Technische Universität Dresden
Center for Systems Biology Dresden
MPI-CBG, Dresden

Pietro Incardona
Technische Universität Dresden
Center for Systems Biology Dresden
MPI-CBG, Dresden

Paul Hunt
Technische Universität Dresden
Center for Systems Biology Dresden
MPI-CBG, Dresden

Guido Reina
Visualization Research
Center, University of
Stuttgart

Steffen Frey
University of Groningen

Stefan Gumhold
Technische Universität Dresden

Ulrik Günther
CASUS, Görlitz
Center for Systems Biology Dresden
MPI-CBG, Dresden

Ivo F. Sbalzarini†
Technische Universität Dresden
Center for Systems Biology Dresden
MPI-CBG, Dresden

ABSTRACT

We present a content-adaptive generation and parallel compositing algorithm for view-dependent explorable representations of large three-dimensional volume data. Large distributed volume data are routinely produced in both numerical simulations and experiments, yet it remains challenging to visualize them at smooth, interactive frame rates. Volumetric Depth Images (VDIs), view-dependent piece wise-constant representations of volume data, offer a potential solution: they are more compact and less expensive to render than the original data. So far, however, there is no method to generate such representations on distributed data and to automatically adapt the representation to the contents of the data. We propose an approach that addresses both issues by enabling sort-last parallel generation of VDIs with content-adaptive parameters. The resulting VDIs can be streamed for display, providing responsive visualization of large, potentially distributed, volume data.

Index Terms: Human-centered computing—Visualization—Visualization theory, concepts and paradigms Human-centered computing—Visualization—Visualization techniques

1 INTRODUCTION

Scientific simulations and experimental measurement devices generate increasingly large scalar field data. For a growing number of applications of scientific exploration, visualization at high, consistent frame rates and low latency is crucial to providing better scientific intuition and interactivity. Compute clusters may be used to accelerate rendering of large data, distributing the data and parallelizing the calculations among processors, but consistent, high frame rates are difficult to achieve due to the time-consuming raycasting procedure and the remote rendering setup requiring communication across a network.

Here, we propose the use of view-dependent piecewise-constant representations of volume data to decouple interactive viewpoint changes and zooming from network latency and distributed volume raycasting. These representations are generated by dividing the volume-rendering integral along each ray into chunks that store cumulative color and opacity. The resulting representation can be

much smaller than the volume data [11], can be compressed and streamed efficiently [10], and recent work has shown that it can be rendered at high frame rates, providing high-fidelity approximations near the viewpoint from which it was generated [12]. However, there currently exists no method to generate such representations on distributed volume data. Moreover, discretizing the volume-rendering integral requires a data and transfer-function dependent parameter, which so far had to be tuned manually to generate accurate representations.

We present a sort-last parallel generation approach for view-dependent representations of distributed volumes. We further introduce an automatic way of determining the discretization parameter, which allows us to do so independently for each ray, resulting in a content-adaptive representation of the data. We choose the Volumetric Depth Image (VDI) [11] as the view-dependent representation. VDIs are generated on each processing element on its volume domain in parallel—we call these “sub-VDis”—and we present an efficient algorithm to composite them in parallel into a single VDI. We further present an algorithm to perform an efficient parameter search for the discretization of the rendering integral into chunks and apply it at both stages of the distributed generation, thereby eliminating the need for manual intervention. We design the compositing algorithm such that it can adapt to arbitrary, potentially non-convex domain decompositions, as may arise, for example, in *in situ* visualization of distributed simulations.

We implement and benchmark our method on real-world datasets. We show that our content-adaptive parameter search for discretizing the rendering integral produces more accurate representations than generation criteria that has been used in previous work. We test the parallel compositing algorithm for accuracy and scalability, showing that it can be used to enable responsive visualization at high frame rates for large, potentially distributed volume data. We implement our method as an extension of an existing open-source visualization library *scenery* [13].

In particular, we contribute the following:

- We propose the use of view-dependent piecewise-constant volume representations, such as VDIs, for interactive visualization of distributed volumes at high, consistent frame rates.
- We propose an efficient parallel compositing algorithm for scalable sort-last generation of VDIs over distributed data.
- We propose a method to automatically discretize the volume integral for each ray by performing a parameter search, enabling content-adaptive representations.

*e-mail: aryaman.gupta@tu-dresden.de

†e-mail: ivo.sbalzarini@tu-dresden.de

2 RELATED WORK

2.1 Distributed Volume Rendering

Volume rendering is widely used for the visualization of 3D scalar fields. Soon after the volume raycasting algorithm was first presented by Levoy [18], parallel volume visualization began to receive research interest [21, 23] with the purpose of achieving interactive visualization by distributing the data and parallelizing the rendering calculations. Recent work in parallel volume rendering has focused on achieving efficient rendering at high degrees of parallelism and for large data sizes [1, 6, 14].

A commonly used strategy for parallel volume rendering is sort-last rendering [14, 22, 25]. There, the volume data are distributed among the n processes taking part in the rendering. Each process performs a front-to-back raycasting on its data, producing a full-resolution sub-image. The sub-images from the various processes are then composited into a single image corresponding to the overall data.

Cavin et al. [4] provide a theoretical comparison of some of the algorithms used for compositing the sub-images. Perhaps the simplest is the direct-send algorithm [8], where the image is divided among the n processes such that each process is responsible for compositing $1/n$ of the total pixels in the final image. For this, each process receives fragments of images from all other processes, corresponding to the part of the final image that it “owns”. Peterka et al. [25] used the direct-send approach in their study of parallel volume rendering on an IBM Blue Gene/P system. Other frequently used compositing algorithms include the binary-swap algorithm [17], which uses a tree data structure with pairs of processes communicating for compositing at every node of the tree, and the hybrid radix- k compositing algorithm [24], which combines the direct-send and binary-swap algorithms, offering configurable parameters for optimization on different hardware architectures. Recent work [19] has aimed to optimize interactivity in distributed visualization by compressing the image data on the GPU before compositing, but responsive visualization with distributed rendering remains a challenge due to network latency between the user and the distributed cluster.

2.2 Explorable Image Representations

Shade et al. [28] introduced the view-dependent Layered Depth Image representation, storing multiple pixels along each line of sight, enabling deferred rendering of surface and geometry data. Stone et al. [30] rendered omnidirectional stereoscopic images of molecular dynamics simulations on remote compute clusters. The images were streamed and reprojected locally at frame rates that enabled Virtual Reality (VR). However, omnidirectional stereoscopic images require warping to prevent distortions [29], which requires depth information and therefore cannot be applied to volume data. For reprojecting volume data, Zellmann et al. [32] transmitted a single depth layer along with the color buffer from the remote rendering server and provided a number of heuristics to create the depth buffer. While the use of a single depth value per pixel creates small message sizes, it is not conducive to producing high-quality reprojections, and holes may occur where rays do not intersect the depth layer. This has been addressed by view-dependent piecewise-constant volume representations, such as the Volumetric Depth Image (VDI), which produce a continuous representation of the volume by storing multiple layers and composited color and opacity in-between. These representations are described in more detail in Sect. 2.3.

Exploratory visualization of numerical simulations was also done post-hoc using the Cinema [2] database, which stores images generated *in situ* using a range of visualization parameters, including different camera viewpoints. All parameters, including viewpoints, however, must be specified in advance, and the database becomes large if many viewpoints are required. Our approach, on the other hand, generates a compact VDI at regular time intervals, which can

be streamed to enable approximate rendering with full 6 degrees-of-freedom camera viewpoint changes.

2.3 View-Dependent Piecewise-Constant Volume Representations

View-dependent representations of volume data are generated by raycasting the volume and decomposing the volume rendering integral into segments, each of which contain pre-classified composited color and opacity, potentially determined using global lighting techniques such as ambient occlusion.

The distinguishing feature of these representations, in comparison to other techniques that compress volume data, is that they produce an exact image when rendered from the original viewpoint of generation, owing to the associativity of the over operator [26] used in alpha-compositing. Rendering from deviating viewpoints involves accumulation over the segments, which is much cheaper than evaluating the full integral [16]. Close approximations to volume rendering are achieved around the viewpoint of generation [11]. Recent work [12] has presented a raycasting-based rendering algorithm, showing that interactive frame rates are achieved at up to 30 degree deviations about the original viewpoint of generation for full-HD viewport resolution.

Previous work in generating view-dependent representations has proposed a variety of strategies to determine the size and extent of the segments generated along the rays. Brady et al. [3] use constant-size segments in each ray, which leads to segments containing composited color and opacity over potentially highly heterogeneous samples, hampering the quality of rendering from a different viewpoint. Lochmann et al. [20] create segments of constant opacity by determining the total transmittance along each ray and partitioning that equally among the segments. This, however, does not account for potentially varying color values within the segments. Frey et al. [11] proposed the Volumetric Depth Image (VDI), which uses homogeneity as a criteria for the creation of segments, accumulating a sample into a segment unless it differs from the segment by more than a pre-defined sensitivity parameter γ . They also permit empty regions between segments if transparent samples are found. Due to these desirable properties, we choose to build upon the VDI representation in our work, albeit replacing the manually defined constant γ with an automated per-ray search. We also propose a sort-last parallel generation technique for view-dependent representations, such as the VDI.

3 THE VOLUMETRIC DEPTH IMAGE (VDI)

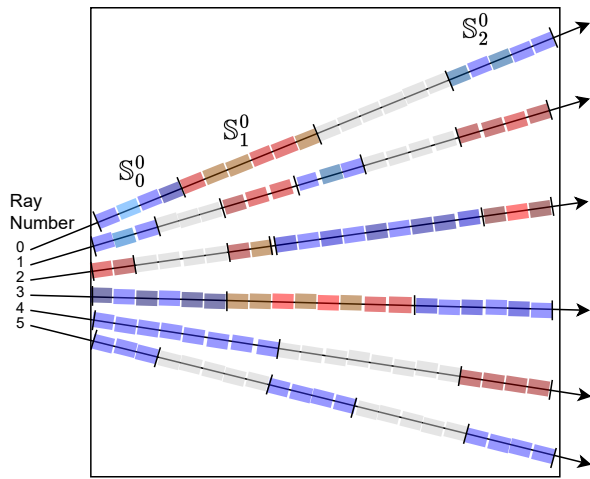
Frey et al. proposed the Volumetric Depth Image [11] as a view-dependent representation of volume data. They call the segments generated along each ray *supersegments*. Each supersegment \mathbb{S} is represented by its front and back faces, $f(\mathbb{S})$ and $b(\mathbb{S})$, and its color and opacity, $C(\mathbb{S})$ and $\alpha(\mathbb{S})$.

Each ray (x, y) cast into the volume creates a so-called *list* \mathbb{L}_{xy} of supersegments \mathbb{S}_j^{xy} where j represents the index of the supersegment in the list (Fig. 1a). The total number of lists created, $|\mathbb{L}|$, corresponds to the viewport resolution the VDI is generated on, i.e. $|\mathbb{L}| = wh$ where w is the width of the viewport and h the height.

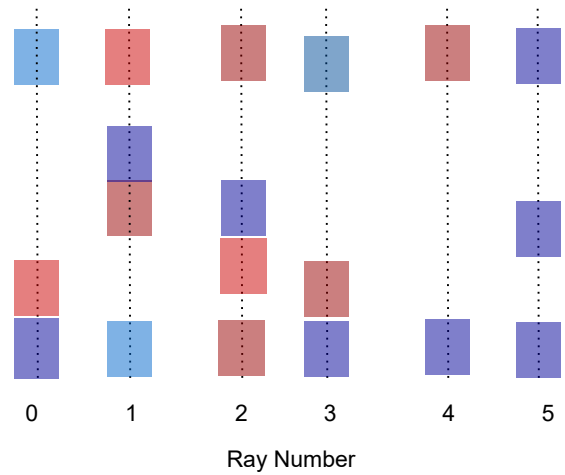
The decomposition of the volume rendering integral into supersegments is governed by a termination criterion τ , which depends on a sensitivity parameter γ . Samples along each ray are merged into a supersegment until

$$\tau : \gamma > \|C(\mathbb{S})\alpha(\mathbb{S}) - C'\alpha'\|_2, \quad (1)$$

where C' and α' are the color and the length-adjusted transmittance of the next sample. In words, a sample along the ray is merged into the current \mathbb{S} unless it differs from the pre-multiplied color of \mathbb{S} by more than γ , in which case a new \mathbb{S} is started. This criterion τ therefore generates homogeneous \mathbb{S} that are important for generating high-quality approximated renderings from changed viewpoints.



(a) Generation of a VDI. Samples collected along rays cast into the volume are partitioned into neighborhoods of similarity called supersegments. Empty spaces are not included.



(b) A VDI: A list of supersegments per-raycast into the volume. Each supersegment is represented by its start and end depths along the ray, and the color and opacity composited within the depth interval

Figure 1: (a) The process of generating a VDI [11] and (b) the VDI representation.

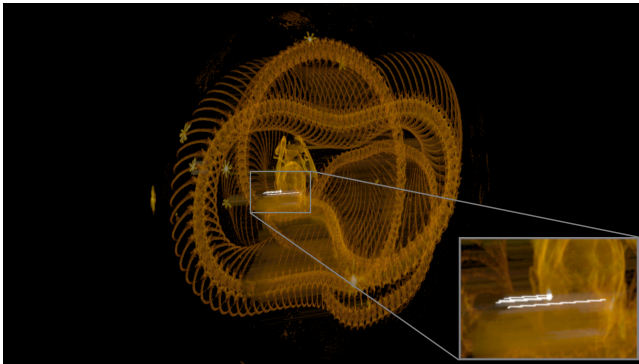


Figure 2: A sample VDI rendering of the Kingsnake dataset showcasing a smearing artefact that results from a low γ value.

The sensitivity parameter γ , however, must be manually selected and is constant across rays. Tuning γ depends on the dataset, transfer function, and colormap. The VDI rendering produced is highly sensitive to the choice of γ , making its manual determination a matter of trial and error. If γ is too low, more supersegments would be generated than the fixed per-list maximum N_S . Then, the last supersegment is forced to accumulate all remaining samples until the ray terminates, leading to “smearing” artefacts in the rendering, as illustrated in Fig. 2. If γ is too high, not enough supersegments are generated, and quality of reprojection is hampered. Moreover, selecting a constant γ for the entire VDI can lead to suboptimal results for heterogeneous datasets.

4 CONTENT-ADAPTIVE AUTOMATIC GENERATION OF SUPERSEGMENTS

Our proposed method retains the homogeneity criteria of Frey et al. [11] (Equation 1), but determines the sensitivity parameter γ automatically and independently for each ray. A maximum of N_S supersegments are generated per list.

Algorithm 1 explains the method used to determine γ . Leveraging the fact that the number of supersegments produced decreases monotonically with increasing γ , algorithm 1 performs an iterative

bisection search between the highest and lowest possible threshold values, using the number of supersegments produced for a given value of γ to adjust γ for the next iteration. Since the distance metric in Equation 1 is an L_2 distance between pre-multiplied color vectors with 3 elements each, the highest possible threshold value is $\sqrt{3}$ and the lowest is 0. Each iteration of the search samples the volume along the ray to determine the number of supersegments generated for a given γ (Line 7).

Since several iterations may be required to determine a γ that generates exactly N_S supersegments, a tolerance of up to δ less supersegments than N_S is permitted, but never more than N_S as this would lead to either the “smearing” artefact mentioned above or to skipping the additional supersegments entirely. In experiments, we found a δ value of 15% of N_S to provide a good trade-off between generation performance and rendering quality. With most datasets and transfer functions, empty regions in volumes are common. To eliminate rays that pass through empty or homogeneous regions, we initialize γ with a small positive value (Line 3). If the first iteration of supersegment generation creates less supersegments than N_S , it implies that the samples along the ray are homogeneous. The ray can therefore terminate, generating either one or zero supersegments depending on whether the region was homogeneous or empty, thereby freeing up computational resources for other rays. The search also terminates when the search space reduces below a small ϵ , selecting the high end of the range as γ , which is guaranteed to produce less supersegments than N_S and therefore prevent smearing, unless it would produce 0 supersegments (line 10). In our experiments, we set ϵ to 10^{-6} . The value of γ produced by algorithm 1 is then used by the ray to generate its list \mathbb{L} .

Performing multiple sampling passes through the volume to determine γ has obvious performance overhead, but it allows the VDI generation to automatically adapt to different datasets and varying transfer functions and color maps. It also generates different values of γ per ray, which yields higher-quality renderings than a globally constant γ , as shown in Table 2.

The parameter N_S controls the performance vs. quality trade-off: Higher values of N_S lead to better rendering quality at lower performance. A constant value of N_S across \mathbb{L} gives the VDI a regular 3D structure in memory, which simplifies the data structure and its generation on distributed data.

Algorithm 1: Determining the supersegment termination parameter γ using an iterative bisection search

```

1 low  $\leftarrow$  0
2 high  $\leftarrow$   $\sqrt{3}$ 
3  $\gamma \leftarrow$  0.00001
4 firstIteration  $\leftarrow$  TRUE
5 found  $\leftarrow$  FALSE
6 while !found do
7   n  $\leftarrow$  numSupersegmentsGenerated( $\gamma$ )
8   if  $\text{abs}(\text{high}-\text{low}) < \epsilon$  then
9     found  $\leftarrow$  TRUE
10     $\gamma \leftarrow$  ((n==0) ? low : high)
11  else if  $n > N_S$  then
12    low = high
13  else if  $n < N_S - \delta$  then
14    high = low
15  else
16    found  $\leftarrow$  TRUE
17  end
18  if firstIteration then
19    firstIteration  $\leftarrow$  FALSE
20    if  $n < N_S$  then
21      found  $\leftarrow$  TRUE
22    end
23  end
24  if !found then
25     $\gamma \leftarrow$  (low + high) / 2
26  end
27 end
28 return  $\gamma$ 

```

4.1 Handling Transparent Samples

Similar to Frey et al. [11] we only begin supersegments at non-transparent samples. While Frey et al. [11] also terminate a supersegment every time a transparent sample is encountered, regardless of the merge criteria τ , we find that this can lead to too much fragmentation along the ray in datasets with high-frequency signals (see Fig. 5). Instead, we terminate supersegments based only on τ , using the iteratively determined γ , recording $b(S)$ as the last non-transparent sample accumulated into S .

5 VOLUMETRIC DEPTH IMAGES OF DISTRIBUTED DATA

We propose a method to generate a VDI representing data that is distributed across Processing Elements (*PE*), e.g., compute nodes in a cluster, GPUs within a node, etc. This extends the content-adaptive automatic supersegment generation of Sect. 4 to work on distributed data. The final VDI then represents the entire volume data in the viewport, though it may lie on multiple *PE*s, and can be transmitted for display.

Our strategy for the parallel generation of VDIs bears similarity to techniques commonly used in the generation of images from distributed data. We follow a sort-last parallel rendering approach [22], in order to achieve scalability with the volume data size, and to conform to arbitrary domain decompositions, e.g. produced by an in-situ simulation. Distributed VDI generation therefore begins with an object-space decomposition, with each *PE* handling a part of the overall volume. Each *PE* generates a VDI at full viewport resolution corresponding to its local data, called a sub-VDI. The sub-VDIs are composited into a single VDI representing the entire volume data using a compositing algorithm that is based on the direct-send algorithm [8]. The compositing stage receives supersegments produced on each *PE* and combines them to produce a total of N_S supersegments per list, ensuring that as little detail as possible is

lost.

5.1 Phase 1: Distributed generation of sub-VDIs

Distributed sub-VDI generation starts from an object-space decomposition. Our approach can adapt to arbitrary domain decompositions, which can be defined externally, for example by an in-situ simulation application running on the *PE*s. As in typical sort-last rendering approaches, a VDI corresponding to the full viewport resolution is generated on each *PE*. All *PE*s share the camera viewpoint, from which rays are cast to generate supersegments.

Any given ray in the view frustum, in general, will pass through the domain of multiple *PE*s, creating supersegments in each of these domains. Using the supersegment generation algorithm from Sect. 4) would therefore require communication and synchronization between all *PE*s at each iteration of the algorithm. Instead, we allow each *PE* to generate N_S supersegments within its domain for each ray. The supersegment generation algorithm can therefore be run in parallel on each *PE*, without any communication or synchronization between *PE*s. Given no communication is required between *PE*s while generating the sub-VDIs, it is important to generate a full N_S on every *PE* in order to correctly discretize the volume integral in cases where all non-transparent samples lie on a single *PE*. We call the supersegments of a sub-VDI as sub-supersegments (S_{sub}).

The output of the first phase of the algorithm is therefore a full-resolution sub-VDI on each *PE*, representing the data held by that *PE*. The work done by a *PE* during sub-VDI generation depends on the size of the volume held by the *PE* as well as the viewport resolution.

5.2 Phase 2: Parallel compositing of sub-VDIs

The goal of the second phase is to composite the distributed sub-VDIs stored on each *PE* to a single VDI representing the entire volume.

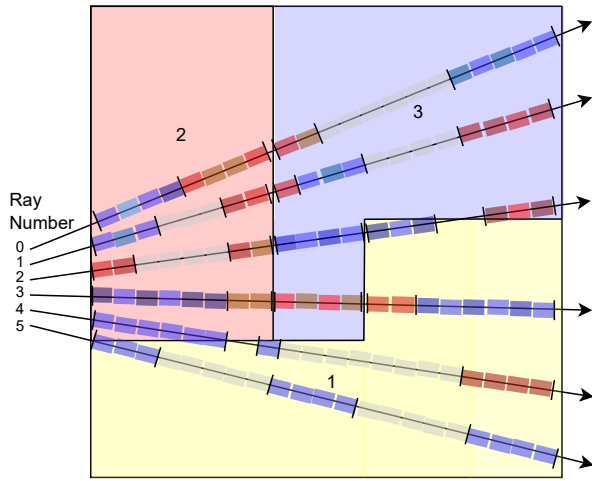
At the end of phase 1, each ray has produced up to N_S sub-supersegments on each *PE* (Fig. 3b). These need to be combined to produce a total of up to N_S supersegments for each ray. The first step is therefore to bring the sub-supersegments for a ray from each *PE* onto a single *PE* where they can be combined.

We design an algorithm based on the direct-send approach for compositing sub-images in distributed volume rendering [23]. In our case, the number of supersegment lists L in the final composited VDI is divided equally among the *PE*s, with each *PE* responsible for producing composited supersegment lists L_{xy} for the pixels in its part of the image space.

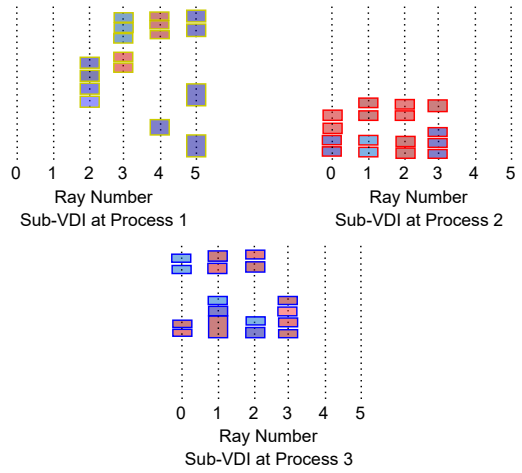
The number of supersegment lists a *PE* needs to produce is therefore $|L|/n$, where n is the total number of *PE*s. For each pixel it is responsible for compositing, a *PE* receives sub-supersegment lists from all *PE*s, including itself. Each *PE* then holds n lists for each pixel it is responsible for compositing. The process of combining the sub-supersegments from the n input lists can be formulated as another supersegment generation task (Section 3), performed by raycasting through the sub-supersegments, which are, after all, piecewise constant representations of the original volume. We can therefore treat each sub-supersegment as a sample along the ray.

The sampling procedure along the ray then requires determining the order in which the sub-supersegments lie along the ray. The sub-supersegments in any list cannot be assumed to be contiguous. There may be gaps in depth between consecutive sub-supersegments when the ray passes into the domain of another *PE*, before returning to the first *PE*. In Fig. 3a, for instance, ray 2 traverses sub-supersegments from *PE* 1, which are to be placed in-between sub-supersegments from *PE* 3.

Each input list contains sub-supersegments in sorted order, since it was created by front-to-back raycasting. Therefore, to determine the next supersegment in a list, the depths of the front-most



(a) Generation of a Distributed VDI. The domain is decomposed among three processing elements (PE), and supersegments are generated by raycasting in parallel on each PE . No synchronisation or communication between PE s is required.



(b) A Distributed VDI: A set of sub-VDIs, one on each PE .

Figure 3: (a) The process of generating a Distributed VDI and (b) the Distributed VDI representation.

sub-supersegments of all input lists are compared, and the sub-supersegment with the lowest starting depth is selected as the next sample along the ray, before being popped off its list.

Algorithm 2 details the procedure of raycasting through sub-supersegments \mathbb{S}_{sub} and combining them into homogenous supersegments \mathbb{S} . Since the sub-supersegments are each of different lengths, the process of raycasting through them is analogous to volume raycasting with irregular step size. The transmittance obtained from sub-supersegment is the transmittance stored in the sub-supersegment, corrected by its length [9] as:

$$\tilde{\alpha} = 1 - (1 - \alpha)^l \quad (2)$$

where $\tilde{\alpha}$ is the adjusted transmittance, α is the transmittance stored in the sub-supersegment, and l is the length of the sub-supersegment.

Raycasting thus steps through the sub-supersegments from all input lists. Empty spaces between \mathbb{S}_{sub} are treated as transparent samples along the ray (lines 17-21 of algorithm 2) with lengths equal to the total empty space between the \mathbb{S}_{sub} . At each sample, the sub-supersegment can either be merged with the previous supersegment, or can begin a new one. This is determined using the same criterion τ (Equation 1) as before and therefore requires determining another γ that leads to the generation of $\mathbb{N}_{\mathbb{S}}$ total supersegments. This is again done per-ray using algorithm 1.

Since the number of supersegments in the list produced is limited to $\mathbb{N}_{\mathbb{S}}$, combining the n input lists into one output list is $O(n)$, where n is the number of PE s. The number of output lists produced by each PE , however, decreases linearly with n , as the lists get divided among more PE s. Therefore, the work performed by any PE during phase 2 is independent of the number of PE s and the size of the volume data.

Between phases 1 and 2, communication of sub-supersegment lists between PE s is required. At the end of Phase 1, each PE holds a screen-resolution sub-VDI consisting of $|\mathbb{L}|$ sub-supersegment lists. This is divided into n equal blocks, each containing $|\mathbb{L}|/n = wh/n$ sub-supersegment lists. One such block is sent to every rendering PE , including one to self, in a manner that conforms with the image-space decomposition described above. This is achieved by an `MPI_AllToAll` call. As the number of PE s increases, the number of messages any PE needs to send increases linearly, but the size of each message decreases linearly. At large n , the high number of messages may thus cause latency issues.

At the end of phase 2, each PE holds wh/n supersegment lists of the composited VDI. These are then gathered on the root PE using an `MPI_Gather` call. Once at the root process, the composited VDI can be streamed for (remote) display, potentially after applying compression techniques [10].

5.3 Handling Non-Convex Data Decompositions

A key feature of our compositing method is that it can handle non-convex domain decompositions and therefore work with any application-given data distribution.

A non-convex domain decomposition is one where a ray can intersect the boundary of the domain of a PE in more than two points. Such decompositions occur, e.g., in numerical simulations in complex-shaped simulation domains, where the domain decomposition balances the computations in each sub-domain and the communication overhead across PE s [15], not necessarily producing an equal division of data among PE s. Figure 4 shows such a hypothetical decomposition where the ray shown intersects the boundary between Processes 1 and 2 at points a , b , c , and d . Such situations are challenging for distributed volume rendering, due to the non-commutativity of the `over` operator [26]:

$$a \text{ over } b \neq b \text{ over } a. \quad (3)$$

The color composited along the ray exemplarily shown in Figure 4 is:

$$C = c_a^b \text{ over } c_b^c \text{ over } c_c^d, \quad (4)$$

where c_a^b represents the color composited from points a and b . In general,

$$C \neq c_a^b \text{ over } c_c^d \text{ over } c_b^c. \quad (5)$$

This implies that in non-convex domain decompositions, volume rendering cannot composite color across disjoint segments of a ray without requiring communication or synchronization between the PE s, or redistribution of the volume data.

Our method avoids this problem by generating supersegments that store world-space front and back depth values along the ray. A supersegment necessarily terminates when the ray leaves the domain of a PE . Since supersegments are sorted by their depth values during compositing, subsequent `over` operations are done in the correct order. The supersegments along a ray can therefore be generated

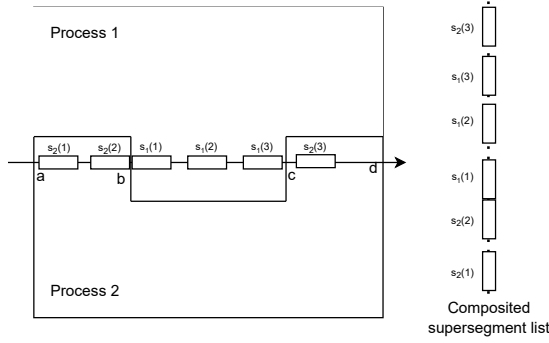


Figure 4: Distributed VDI generation on a non-convex domain decomposition between two processes. The ray shown intersects the domain of Process 2 at four points: a, b, c, d. The sub-supersegments (boxes) are depth-ordered and placed in the correct sequence before being composited into supersegments.

in parallel without synchronization or communication between the *PEs*, as illustrated in Figure 4.

We note that our method includes non-convex distributed volume rendering as a limit case: when generating only a single supersegment per sub-domain intersection, the compositing algorithm can, in addition to placing the supersegments in order, also perform over-operator compositing along the supersegment lists. This effectively performs volume rendering of a plain image on a non-convex domain decomposition without requiring synchronization or communication between *PEs*.

6 IMPLEMENTATION

We have implemented the algorithms described in the previous sections on top of the open-source rendering framework *scenery* [13]. Both sub-VDI generation and VDI compositing are implemented as compute shaders via the Vulkan API. For work distribution in the compute shaders, a local work-group size of 16x16 is used, i.e., the screen space is divided into 2D blocks of that size. Upon raycasting, each ray within the block corresponds to a thread on the GPU, and a single pixel on screen. The image load/store texture used for writing the VDI, which is pre-allocated, with a user-defined maximum number of supersegments. The layout of the texture is $\mathbb{N}_{\mathbb{S}} \times w \times h$, which is somewhat unorthodox, but chosen to enable easy decomposition and fast CPU-side copying for MPI communication. Each VDI consists of two floating-point textures: one for storing color and opacity of supersegments (type RGBA32F), and one for the depth of the supersegments (type R32F). The resulting VDIs have the full resolution of the screen.

The full source code is available under the open-source BSD license and can be found at github.com/scenerygraphics/scenery-insitu.

7 EXPERIMENTAL SETUP

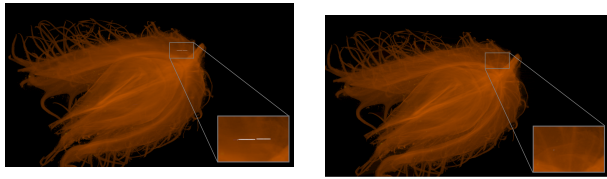
We tested our system on the *alpha-centauri* partition of the Taurus high-performance computer at the Technische Universität Dresden. Each node contains 8 NVIDIA A100-SXM4 GPUs with 40 GB of DRAM each, 2 AMD EPYC 7352 CPUs with 24 cores each, and 1 TB RAM, and runs Red Hat Enterprise Linux version 7.9. C++ code was compiled using GCC 10.3.0. Java code was run using OpenJDK 11.0.2, and OpenMPI version 4.1.1 was used. Rendering of VDIs, performed to verify the quality of VDIs generated, used the recently proposed raycasting method [12] for rendering VDIs, running on an Nvidia RTX 3090 on a workstation with Ubuntu 20.04. Performance of VDI rendering was previously reported on the same hardware setup, and is therefore not reported here. Processes were always

Algorithm 2: Combining sub-supersegments into supersegments

```

/* Combining sub-supersegments along a ray
   into supersegments for a given  $\gamma$  */
1 supersegmentIsOpen  $\leftarrow$  False
2  $f(\mathbb{S}), b(\mathbb{S}) \leftarrow 0$ 
3  $b(\mathbb{S})_r \leftarrow 0$ 
4  $C(\mathbb{S}), \alpha(\mathbb{S}) \leftarrow 0$ 
5 transparent  $\leftarrow$  False
6
/* The front element of all lists is
   initialized to the index of the first
   element */
7 frontIndex[0...n]  $\leftarrow$  1
8 while !samplesComplete do
9    $C(\mathbb{S}_{sub}), \alpha(\mathbb{S}_{sub}), f(\mathbb{S}_{sub}), b(\mathbb{S}_{sub}), p \leftarrow$ 
     findNextSub(frontIndex[])
10  if  $p = -1$  then
11    samplesComplete  $\leftarrow$  True
12  end
13   $l \leftarrow \text{distance}(f(\mathbb{S}_{sub}), b(\mathbb{S}_{sub}))$ 
14   $\tilde{\alpha}(\mathbb{S}_{sub}) = 1 - (1 - \alpha(\mathbb{S}_{sub}))^l$ 
15  if supersegmentIsOpen then
16    if  $f(\mathbb{S}_{sub}) > b(\mathbb{S})$  then
17      transparent  $\leftarrow$  True
18       $C(\mathbb{S}_{sub}), \alpha(\mathbb{S}_{sub}) \leftarrow 0$ 
19       $b(\mathbb{S}_{sub}) \leftarrow f(\mathbb{S}_{sub})$ 
20       $f(\mathbb{S}_{sub}) \leftarrow b(\mathbb{S})$ 
21    end
22     $\widetilde{C}(\mathbb{S}) \leftarrow \frac{C(\mathbb{S})}{\alpha(\mathbb{S})}$ 
23     $l_s \leftarrow \text{distance}(f(\mathbb{S}), b(\mathbb{S}))$ 
24     $\widetilde{\alpha}(\mathbb{S}) = 1 - (1 - \alpha(\mathbb{S}))^{l_s}$ 
25    if  $\gamma < \|\widetilde{C}(\mathbb{S})\widetilde{\alpha}(\mathbb{S}) - C(\mathbb{S}_{sub})\alpha(\mathbb{S}_{sub})\|_2$  then
26      newSupersegment  $\leftarrow$  True
27    end
28    if newSupersegment || samplesComplete then
29      /* Closing  $\mathbb{S}$ . If  $\gamma$  was the final
30       value determined by algorithm 1,
31       store  $\mathbb{S}_{sub}$  */
32      numTerminations  $\leftarrow$  numTerminations + 1
33    else
34       $C(\mathbb{S}) \leftarrow C(\mathbb{S}) + (1 - \alpha(\mathbb{S})) * C(\mathbb{S}_{sub}) * \alpha(\mathbb{S}_{sub})$ 
35       $\alpha(\mathbb{S}) \leftarrow \alpha(\mathbb{S}) + (1 - \alpha(\mathbb{S})) * \alpha(\mathbb{S}_{sub})$ 
36       $b(\mathbb{S}) \leftarrow b(\mathbb{S}_{sub})$ 
37      if !transparentSample then
38         $b(\mathbb{S})_r \leftarrow b(\mathbb{S}_{sub})$ 
39      end
40    end
41  end
42  if !supersegmentIsOpen & !transparent then
43    supersegmentIsOpen  $\leftarrow$  True
44     $f(\mathbb{S}) \leftarrow f(\mathbb{S}_{sub})$ 
45     $b(\mathbb{S}), b(\mathbb{S})_r \leftarrow b(\mathbb{S}_{sub})$ 
46     $C(\mathbb{S}) \leftarrow C(\mathbb{S}_{sub}) * \alpha(\mathbb{S}_{sub})$ 
47     $\alpha(\mathbb{S}) \leftarrow \alpha(\mathbb{S}_{sub})$ 
48  end
49 end

```



(a) Terminations at each transparent sample.

(b) Terminations determined only by τ .

Figure 5: A VDI rendering at 30° from viewpoint of generation on the Beechnut dataset, comparing the approach terminating supersegments at each transparent, vs. not doing so. Both VDIs were generated using an per-ray γ determined using algorithm 1. Smearing artefacts are possible when supersegments are terminated at every transparent sample, as in (a).

distributed in a block manner across nodes, i.e., all 8 GPUs on a node were occupied before using another node, if necessary.

The datasets used for the evaluation are described in Table 1. Kingsnake, Beechnut, and Richtmyer-Meshkov [7] are commonly used visualization datasets. Boneplug is from a PEGASOS-cleared mouse tibia bone marrow plug acquired using lightsheet fluorescence microscopy [5]. Finally, the rotating stratified turbulence dataset (Rotstrat) shows the temperature field from a direct numerical simulation of turbulent fluid flow [27]. In each case, we used a simple domain decomposition, splitting the volumes along their z -axis equally among PE s.

8 RESULTS AND EVALUATION

We compare the quality of VDIs generated using our content-adaptive supersegment generation approach (Sect. 4), which uses a different automatically determined value of γ for each ray, against the original approach of Frey et al. [11], which used a manually tuned constant value of γ across all rays. In order to select a suitable global value of γ for comparison, we run our iterative content-adaptive algorithm (algorithm 1), producing a unique γ at each ray, and then choose the median γ over all the rays that passed through non-empty regions of the volume as the global γ value.

Table 2 reports the results of the comparison, performed on a VDI of viewport resolution 1920×1080 , with $N_S = 20$. VDIs generated from a viewpoint V_O are rendered at different degrees of rotation around V_O . Comparison is performed in each case to the ground-truth volume rendering, and uses the SSIM [31] metric, where identical images result in a value of 1.0. We observe that our content-adaptive approach of selecting a unique γ per ray produces better or equal results in all cases. The difference in rendering quality increases with increasing angle deviation around V_O . The exception is the Beechnut dataset, where the selected global γ seems to be almost optimal.

Our supersegment generation approach also differs from Frey et al. [11] in how transparent samples along the ray are handled: We do not terminate a supersegment at each transparent sample, but allow the termination to be governed only by τ (Equation 1). Figure Fig. 5 provides a comparison between the two approaches for the Beechnut dataset. In both cases, a γ is determined per-ray using algorithm 1, but in the case of Fig. 5a, supersegments are terminated at every transparent sample, while Fig. 5b uses our proposed approach of terminating based on τ . A smearing artefact is visible in Fig. 5a, because some rays exceed their supersegment budget during generation, due to too many terminations caused by transparent samples. Our approach avoids the smearing artefact by merging across transparent samples, if necessary, and better utilizing the supersegment budget.

Next, we evaluate the run-time of the content-adaptive VDI generation approach by measuring the time taken to generate a single VDI

on a single GPU for different VDI and dataset resolutions. To test scalability with volume size, we produce a downsampled version of the Boneplug dataset with a resolution of $5154 \times 1874 \times 1839$ (uint 16), producing a volume that just fits into the 40 GB DRAM of the Nvidia A100 GPU. Table 3 reports the mean times for the generation of a single VDI over 144 iterations. Timings reported include the kernel time as well as the time required to transfer the generated VDI from the GPU to the CPU. Each subsequent VDI is generated for a 5° rotation of the dataset, with the camera always pointing at the center of the dataset, until two full revolutions are completed, for a total of $\frac{360}{5} \cdot 2 = 144$ successive VDI generations.

Generation times scale as expected with the volume and viewport resolution: larger numbers of voxels require more memory samples at each iteration of the γ search, and high viewport resolutions launch more rays that need to sample the volume. Slightly unexpected is the observation that VDIs with $N_S=15$ took longer to generate than VDIs with $N_S=30$, despite the fact that $N_S=30$ VDIs are slower to write to for the kernel, and slower to fetch from the GPU. Analysis revealed that this is caused by our γ -search algorithm converging to a suitable value in fewer iterations for $N_S=30$ VDIs than for the $N_S=15$ VDIs.

Next, we evaluate the accuracy of supersegment compositing (algorithm 2). We consider datasets that fit the memory of a single GPU and compare VDIs generated on a single GPU, where no compositing is performed, with VDIs generated with the data distributed over multiple GPUs. To eliminate potential bias in the results caused by the domain decomposition splitting the data among PE s only along along the z -dimension, we choose two different viewpoints for VDI generation: V_1 and V_2 . V_2 is a 90° rotation of the camera around the dataset from V_1 . The camera points at the center of the dataset in both cases. VDIs are then rendered for different viewpoints about the viewpoint of generation, and quality is compared against ground-truth volume rendering. Table 4 reports the results.

We find that the quality of the images produced by VDI rendering remains similarly high for VDIs generated on multiple GPUs as for a VDI generated on a single GPU, indicating that our compositing algorithm is formulated and implemented correctly.

Next, we evaluate the performance of our parallel sort-last compositing algorithm, including the MPI communication involved therein, i.e., Phase 2 (Sect. 5.2) of our parallel VDI generation. VDIs were generated on the Richtmyer-Meshkov dataset. We note that the performance of this phase does not scale with the size of the volume, only with the resolution of the VDI. The dataset filled the viewport to ensure accurate measurement of the compositing algorithm, and every subsequent VDI was generated with a revolution of 10° about the data. Results are averaged over 100 successive VDI generations. An `MPI.Barrier` was placed before the MPI calls. Results are reported for in Fig. 6 for the three stages of Phase 2 (Sect. 5.2).

We observe that the overall compositing time increases with increasing number of GPUs, due to an increase in the time spent in the `MPI.AllToAll`. Our implementation allocates and transmits full-resolution 3D sub-VDIs at each PE , which leads to the total data to be communicated increasing linearly with the number of PE s.

Finally, we evaluate the overall VDI generation and compositing for the large Boneplug and Rotstrat datasets. Performance is reported in Fig. 7. Once again, the camera revolved around the dataset at 10° steps, and results are averaged over 100 successive VDI generations. We observe differing performance and scalability for the two datasets, which is due to the sub-VDI generation time being larger for the Rotstrat dataset. This is at least partially due to the difference in shape between the two datasets; we selected camera viewpoints such that the entire data was in the viewport. In the case of the Rotstrat dataset, this meant that the data filled the viewport along both dimensions, while the Boneplug dataset left the y -dimension partially empty due to its much larger length along

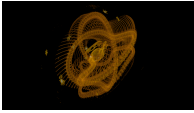
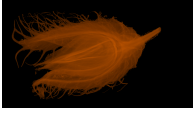
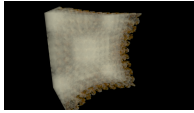
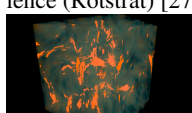
Kingsnake 	Beechnut 	Richtmyer-Meshkov [7] 	Boneplug [5] 	Rotating stratified turbulence (Rotstrat) [27] 
1024×1024×795, 8bit, 795 MiB	1024×1024×1546, 16bit, 3092 MiB	2048×2048×1920, 8bit, 7680 MiB	25762×9366×9189, 16bit, 8.2 TiB; downsampled to 8588×3122×3064, 16bit, 156 GiB	4096×4096×4096, 32bit, 256 GiB; converted to uint 16, 128 GiB

Table 1: Description of the datasets used.

VDI Generation Method	Kingsnake		Beechnut		Richtmyer-Meshkov	
	S 5°	S 30°	S 5°	S 30°	S 5°	S 30°
Orig.	0.971	0.931	0.989	0.986	0.981	0.979
Ours	0.986	0.971	0.992	0.986	0.985	0.986

Table 2: Comparing our content-adaptive supersegment against the original method of Frey et al. [11]. SSIM values of the rendering of the resultant VDI are compared at 5- and 30-degree rotation, with respect to ground truth volume rendering.

	1280x720 Ns = 15	1280x720 Ns = 30	1920×1080 Ns = 15	1920×1080 Ns = 30
Kingsnake	0.16	0.12	0.27	0.25
Beechnut	0.35	0.31	0.74	0.62
Richtmyer Meshkyov	0.76	0.71	1.37	1.25
Boneplug (34 GB)	1.75	1.72	2.94	2.63

Table 3: Wall-clock time (mean, in seconds) to generate a single VDI.

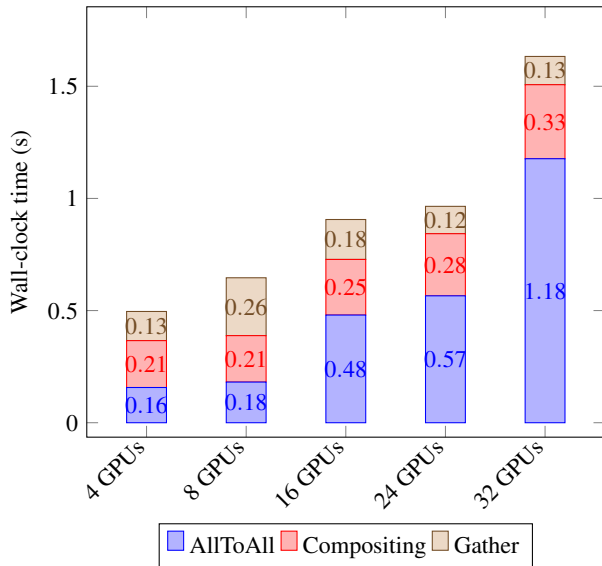


Figure 6: Wall-clock time of the three stages involved the parallel compositing of a VDI with viewport resolution 1920×1080, $N_S=20$, for different numbers of GPUs.

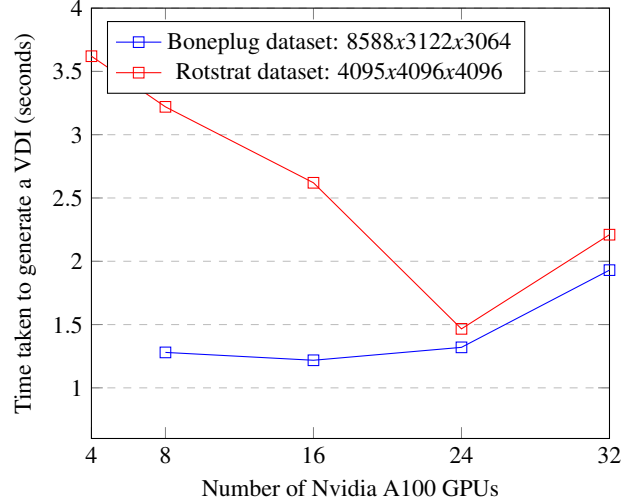


Figure 7: Generation time of 1920×1080 VDIs with $N_S=20$ at varying degrees of parallelism and data sizes.

x. The difference is particularly evident at small number of GPUs, where the sub-VDI generation time dominates. At higher number of GPUs, we observe that the MPI_AllToAll time begins to dominate, as the data is divided into smaller chunks, and communication increases (Fig. 6).

We also evaluate the quality of the final VDIs generated on the Boneplug and Rotstrat datasets. Results are reported in Table 5, showing that image quality is maintained on VDIs generated on the largest of the datasets tested. Fig. 8 provides visual comparison.

9 DISCUSSION AND CONCLUSIONS

We have presented algorithms for content-adaptive generation of Volumetric Depth Images [11] on distributed volume data and their parallel compositing. This enables responsive visualization of large distributed volume data on GPU clusters. We introduced a per-ray iterative search for the supersegment termination criterion in order to enable automatic generation of optimally homogeneous supersegments. We proposed a sort-last parallel generation approach to scale to large volume sizes. Full resolution VDIs are generated at each PE and composited in parallel. No communication or transfer of the volume data is required. We also proposed a parallel compositing algorithm where the supersegments generated on each PE are treated as samples of various lengths and accumulated into a combined final VDI for display.

Our benchmarks have shown that using a per-ray value of γ , instead of a global value as originally proposed by Frey et al. [11], produces VDIs that provide better or equal quality rendering approxi-

Dataset		1 GPU			4 GPUs			32 GPUs		
		5°	15°	30°	5°	15°	30°	5°	15°	30°
Kingsnake	V ₁	0.986	0.981	0.971	0.982	0.976	0.967	0.985	0.980	0.969
	V ₂	0.986	0.981	0.974	0.986	0.981	0.974	0.984	0.980	0.972
Beechnut	V ₁	0.993	0.990	0.986	0.992	0.990	0.986	0.991	0.989	0.985
	V ₂	0.991	0.983	0.973	0.991	0.984	0.973	0.991	0.983	0.972
Richtmyer-Meshkov	V ₁	0.985	0.985	0.986	0.985	0.985	0.986	0.984	0.984	0.984
	V ₂	0.985	0.984	0.986	0.985	0.984	0.986	0.984	0.983	0.985

Table 4: The SSIM quality, with respect to ground truth volume rendering, for VDIs generated using varying number of Nvidia A100 GPUs. VDIs generated on 4 and 32 GPUs are composited using our compositing algorithm (Sect. 5.2), while VDIs generated on 1 GPU do not undergo compositing. All VDIs were of viewport resolution 1920×1080 , with $N_S = 20$.

Dataset	10°	20°	30°
Boneplug	0.978	0.975	0.972
Rotstrat	0.982	0.978	0.975

Table 5: SSIM image similarity between 1920×1080 , $N_S = 20$ VDIs generated on 16 GPUs, and ground truth volume rendering, at varying degrees of rotation about the viewpoint of generation.

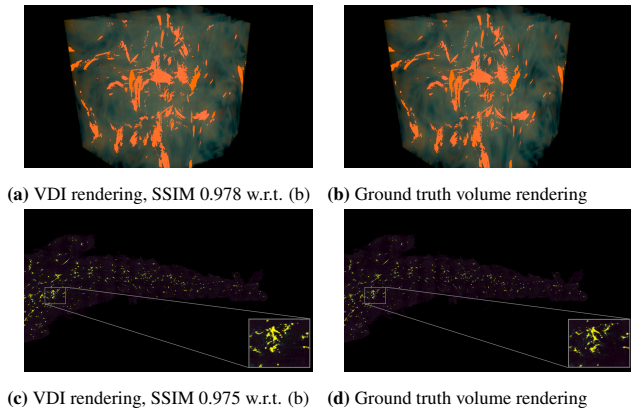


Figure 8: Visual comparison between ground-truth volume renderings and a VDI generated on 16 GPUs at 20° viewpoint deviation.

mations (Table 2). It also enables VDIs to be generated automatically, eliminating the need for manual parameter tuning, which would be hard in a distributed setup. Further, our benchmarks showed that the proposed compositing algorithm maintains the quality of the VDI (Table 4). The sort-last parallel generation approach enables the generation of VDIs representing more than 100 gigabytes of volume data in less than 2 seconds (Fig. 7), depending on the degree of parallelism.

We evaluated compression of the VDI and found that the multi-threaded LZMA (compared to Brotli, gzip, and Zstd) performed best, yielding combined compression and decompression times of about one second (tested on an Apple M1 Max using 10 CPU threads), reducing the total VDI size to about 80 MiB for a full-HD viewport resolution and $N_S = 20$. The generated VDI therefore provides a compact representation of the volume that can be streamed for responsive visualization with 6 degrees of freedom for the camera movement. Recent work [12] has shown that full-HD VDIs can be rendered at between 13 and 84 fps for viewpoint deviations between 5° and 30° . While rendering of the VDI maintains responsive visualization at the user’s display, a new VDI could be generated from the user’s latest viewpoint and streamed when ready, maintaining interactivity and accuracy.

We performed benchmarks on volume data loaded from disk,

which allowed us to analyze the performance of the VDI generation in isolation. However, we also see this as a potential solution for *live in situ* visualization of numerical simulations. The time taken to generate a VDI (Fig. 7) is shorter or comparable to the time steps of typical computer simulations, implying that visualization at full temporal resolution would be possible. In comparison to the Cinema technique [2], which generates a database of images to enable interactive visualization, the VDI does not require the desired viewpoints to be pre-defined, and it allows for full 6 degrees-of-freedom user navigation. It also is generated from only one viewpoint and is therefore potentially faster and more compact than the larger number of images that would need to be generated for a database to enable navigation with 6 degrees of freedom. In this sense, the present approach is complementary to Cinema. While Cinema enables post-hoc exploration of a wide array of visualization parameters, we focus on rapid viewpoint changes in a *live in situ* use case with potentially remote display clients.

We note that while the present content-adaptive supersegment generation approach was efficient here (Table 3), it may run into limitations when the VDI is to be generated with more complex lighting models, such as global ambient occlusion. Then, each step of the iterative algorithm would need to perform additional lighting calculations. We also observe that our use of MPI.All.to.All for compositing full-resolution VDIs does not scale to arbitrarily large numbers of GPUs (Fig. 6). Ensuring theoretical scalability would likely require the use of Active Pixel encoding for the sub-VDIs, as for example implemented in IceT [19].

Nevertheless, we believe the methods we have proposed represent a significant advance in the field of view-dependent volume representations, such as the VDI, and their use on large, distributed data. We see our method finding use in interactive applications, such as the computational steering of distributed numerical simulations.

ACKNOWLEDGMENTS

This work was supported by the Center for Scalable Data Analytics and Artificial Intelligence (ScaDS.AI) Dresden/Leipzig, funded by the Federal Ministry of Education and Research (Bundesministerium für Bildung und Forschung, BMBF), and by the Center for Advanced Systems Understanding (CASUS), which is financed by Germany’s Federal Ministry of Education and Research (BMBF) and by the Saxon Ministry for Science, Culture and Tourism (SMWK) with tax funds on the basis of the budget approved by the Saxon State Parliament. We thank Prof. Kevin Dean, Lyda Hill Department of Bioinformatics, University of Texas Southwestern, for his support in sharing the Boneplug dataset. We acknowledge the Computer-Assisted Paleoanthropology group and the Visualization and Multi-Media Lab at University of Zurich (UZH) for the acquisition of the μ CT Beechnut dataset. We acknowledge the University of Texas High-Resolution X-ray CT Facility (UTCT) for the acquisition of the Kingsnake dataset.

REFERENCES

- [1] T. Biedert, K. Werner, B. Hentschel, and C. Garth. A Task-Based Parallel Rendering Component For Large-Scale Visualization Applications. In A. Telea and J. Bennett, eds., *Eurographics Symposium on Parallel Graphics and Visualization*. The Eurographics Association, 2017. doi: 10.2312/pgv.20171094
- [2] A. Biswas, S. Dutta, J. Pulido, and J. Ahrens. In Situ Data-Driven Adaptive Sampling for Large-Scale Simulation Data Summarization. In *Proceedings of the Workshop on In Situ Infrastructures for Enabling Extreme-Scale Analysis and Visualization*, ISAV '18, p. 13–18. Association for Computing Machinery, New York, NY, USA, 2018. doi: 10.1145/3281464.3281467
- [3] M. Brady, K. Jung, H. Nguyen, and T. Nguyen. Two-phase perspective ray casting for interactive volume navigation. In *Proceedings. Visualization '97 (Cat. No. 97CB36155)*, pp. 183–189, 1997. doi: 10.1109/VISUAL.1997.663878
- [4] X. Cavin, C. Mion, and A. Filbois. COTS cluster-based sort-last rendering: performance evaluation and pipelined implementation. In *VIS 05. IEEE Visualization, 2005.*, pp. 111–118, 2005. doi: 10.1109/VISUAL.2005.1532785
- [5] T. Chakraborty, M. K. Driscoll, E. Jeffery, M. M. Murphy, P. Roudot, B.-J. Chang, S. Vora, W. M. Wong, C. D. Nielson, H. Zhang, V. Zhemkov, C. Hiremath, E. D. De La Cruz, Y. Yi, I. Bezprozvanny, H. Zhao, R. Tomer, R. Heintzmann, J. P. Meeks, D. K. Marciano, S. J. Morrison, G. Danuser, K. M. Dean, and R. Fiolka. Light-sheet microscopy of cleared tissues with isotropic, subcellular resolution. *Nature Methods*, 16(11):1109–1113, Nov. 2019. doi: 10.1038/s41592-019-0615-4
- [6] H. Childs, M. A. Duchaineau, and K.-L. Ma. A scalable, hybrid scheme for volume rendering massive data sets. 2006.
- [7] R. H. Cohen, W. P. Dannevik, A. M. Dimits, D. E. Eliason, A. A. Mirin, Y. Zhou, D. H. Porter, and P. R. Woodward. Three-dimensional simulation of a Richtmyer–Meshkov instability with a two-scale initial perturbation. *Physics of Fluids*, 14(10):3692–3709, 2002. doi: 10.1063/1.1504452
- [8] S. Eilemann and R. Pajarola. Direct send compositing for parallel sort-last rendering. 2007.
- [9] K. Engel, M. Hadwiger, J. M. Kniss, A. E. Lefohn, C. R. Salama, and D. Weiskopf. Real-time volume graphics. In *ACM SIGGRAPH 2004 Course Notes*, SIGGRAPH '04, p. 29–es. Association for Computing Machinery, New York, NY, USA, 2004. doi: 10.1145/1103900.1103929
- [10] O. Fernandes, S. Frey, F. Sadlo, and T. Ertl. Space-time volumetric depth images for in-situ visualization. In *2014 IEEE 4th Symposium on Large Data Analysis and Visualization (LDAV)*, pp. 59–65, 2014.
- [11] S. Frey, F. Sadlo, and T. Ertl. Explorable volumetric depth images from raycasting. In *2013 XXVI Conference on Graphics, Patterns and Images*, pp. 123–130. IEEE, 2013.
- [12] A. Gupta, U. Günther, P. Incardona, G. Reina, S. Frey, S. Gumhold, and I. F. Sbalzarini. Efficient raycasting of view-dependent piecewise constant representations of volumetric data, 2022. doi: 10.48550/ARXIV.2206.08660
- [13] U. Günther, T. Pietzsch, A. Gupta, K. I. Harrington, P. Tomancak, S. Gumhold, and I. F. Sbalzarini. scenery: Flexible virtual reality visualization on the Java VM. In *2019 IEEE Visualization Conference (VIS)*, pp. 1–5, 2019. doi: 10.1109/VISUAL.2019.8933605
- [14] M. Howison, E. W. Bethel, and H. Childs. Hybrid parallelism for volume rendering on large-, multi-, and many-core systems. *IEEE Transactions on Visualization and Computer Graphics*, 18(1):17–29, 2011.
- [15] P. Incardona, A. Leo, Y. Zaluzhnyi, R. Ramaswamy, and I. F. Sbalzarini. OpenFPM: A scalable open framework for particle and particle-mesh codes on parallel computers. *Computer Physics Communications*, 241:155–177, 2019.
- [16] A. Kaufman and K. Mueller. *Overview of Volume Rendering*, vol. 7, pp. 127–XI. 12 2005. doi: 10.1016/B978-012387582-2/50009-5
- [17] Kwan-Liu Ma, J. S. Painter, C. D. Hansen, and M. F. Krogh. Parallel volume rendering using binary-swap compositing. *IEEE Computer Graphics and Applications*, 14(4):59–68, 1994.
- [18] M. Levoy. Display of surfaces from volume data. *IEEE Computer Graphics and Applications*, 8(3):29–37, 1988.
- [19] R. Lipinski, K. Moreland, M. E. Papka, and T. Marrinan. GPU-based image compression for efficient compositing in distributed rendering applications. In *2021 IEEE 11th Symposium on Large Data Analysis and Visualization (LDAV)*, pp. 43–52, 2021. doi: 10.1109/LDAV53230.2021.00012
- [20] G. Lochmann, B. Reinert, A. Buchacher, and T. Ritschel. Real-time Novel-view Synthesis for Volume Rendering Using a Piecewise-analytic Representation. In M. Hullin, M. Stamminger, and T. Weinkauff, eds., *Vision, Modeling 'I&' Visualization*. The Eurographics Association, 2016. doi: 10.2312/vmv.20161346
- [21] K.-L. Ma, J. S. Painter, C. D. Hansen, and M. F. Krogh. A data distributed, parallel algorithm for ray-traced volume rendering. In *Proceedings of 1993 IEEE Parallel Rendering Symposium*, pp. 15–22. IEEE, 1993.
- [22] S. Molnar, M. Cox, D. Ellsworth, and H. Fuchs. A sorting classification of parallel rendering. *IEEE Computer Graphics and Applications*, 14(4):23–32, 1994. doi: 10.1109/38.291528
- [23] U. Neumann. Parallel volume-rendering algorithm performance on mesh-connected multicomputers. In *Proceedings of 1993 IEEE Parallel Rendering Symposium*, pp. 97–104, 1993.
- [24] T. Peterka, D. Goodell, R. Ross, H.-W. Shen, and R. Thakur. A configurable algorithm for parallel image-compositing applications. In *Proceedings of the Conference on High Performance Computing Networking, Storage and Analysis*, pp. 1–10. IEEE, 2009.
- [25] T. Peterka, H. Yu, R. Ross, K.-L. Ma, and R. Latham. End-to-end study of parallel volume rendering on the IBM Blue Gene/P. In *2009 International Conference on Parallel Processing*, pp. 566–573. IEEE, 2009.
- [26] T. Porter and T. Duff. Compositing digital images. In *Proceedings of the 11th annual conference on Computer graphics and interactive techniques*, pp. 253–259, 1984.
- [27] D. Rosenberg, A. Pouquet, R. Marino, and P. D. Mininni. Evidence for Bolgiano-Obukhov scaling in rotating stratified turbulence using high-resolution direct numerical simulations. *Physics of Fluids*, 27(5):055105, May 2015. doi: 10.1063/1.4921076
- [28] J. Shade, S. Gortler, L.-w. He, and R. Szeliski. Layered Depth Images. In *Proceedings of the 25th Annual Conference on Computer Graphics and Interactive Techniques*, SIGGRAPH '98, p. 231–242. Association for Computing Machinery, New York, NY, USA, 1998. doi: 10.1145/280814.280882
- [29] A. Simon, R. Smith, and R. Pawlicki. Omnistereo for panoramic virtual environment display systems. In *IEEE Virtual Reality 2004*, pp. 67–79, 2004. doi: 10.1109/VR.2004.1310057
- [30] J. E. Stone, W. R. Sherman, and K. Schulten. Immersive molecular visualization with omnidirectional stereoscopic ray tracing and remote rendering. In *2016 IEEE International Parallel and Distributed Processing Symposium Workshops (IPDPSW)*, pp. 1048–1057, 2016. doi: 10.1109/IPDPSW.2016.121
- [31] Z. Wang, A. Bovik, H. Sheikh, and E. Simoncelli. Image quality assessment: from error visibility to structural similarity. *IEEE Transactions on Image Processing*, 13(4):600–612, 2004. doi: 10.1109/TIP.2003.819861
- [32] S. Zellmann, M. Aumüller, and U. Lang. Image-Based Remote Real-Time Volume Rendering: Decoupling Rendering From View Point Updates. In *International Design Engineering Technical Conferences and Computers and Information in Engineering Conference*, pp. 1385–1394, 08 2012. doi: 10.1115/DETC2012-70811